doi:10.1038/nature09477

S1. Neutron scattering methods

We employed both spin-polarized and unpolarized INS measurements. The use of spin-polarized neutrons was crucial to unambiguously identify the magnetic response reported here, because such neutrons are separately collected according to whether their spins have or have not been flipped in the scattering process, which renders magnetic and nuclear scattering clearly distinguishable.

In our spin-polarized experiment, the spin polarization of incident neutrons can be freely chosen. The primary spin geometry is with incident polarization (**S**) parallel to momentum transfer (**Q**), in which magnetic and nuclear scattering occurs only in the spin-flip and non-spin-flip channels, respectively. The unwanted nuclear scattering is suppressed by a factor of 15 and becomes practically undetectable. Two additional polarization geometries were used to determine the genuine background level. The method employs the principle that neutrons scattered in the spin-flip channel probe magnetic response perpendicular to both **S** and **Q**. The sum of the intensities (I) in the $\mathbf{S}\perp\mathbf{Q}$ (polarization perpendicular to **Q** and in the horizontal scattering plane) and $\mathbf{S}||\mathbf{Z}$ (polarization vertical) geometries should contain the same magnetic signal as in the $\mathbf{S}||\mathbf{Q}$ geometry, but twice the background. Consequently, the quantity $I_{\mathbf{S}\perp\mathbf{Q}} + I_{\mathbf{S}||\mathbf{Z}} - I_{\mathbf{S}||\mathbf{Q}}$ represents only the background (see Fig. 1a).

The spin-polarized experiment was carried out on spectrometer IN20 at the Institute

Laue Langevin (ILL), using a Heusler-Heusler setup (resolution ~10 meV FWHM in the 50–60 meV energy transfer range). Data are presented in Figs. 1a-b, 2a, S3, and S8a. The unpolarized experiments were performed on 2T (Figs. 2b, 3a, and S6) at the Laboratoire Léon Brillouin (LLB), on PUMA (Figs. S4-5 and S8b-d) at the Forschungs-Neutronenquelle Heinz Maier-Leibnitz (FRM II), and on IN8 (Figs. 2c-d and 3a) at ILL. Pyrolytic graphite (PG) analyzers were used in the unpolarized experiments. Together with PG(002) or Cu(200) monochromators, the energy resolution in the 50–60 meV energy transfer range is ~10 meV FWHM or ~5 meV FWHM, respectively. PG filters were used in all measurements to suppress harmonic contamination in the final neutron beam, the energy of which was fixed at 30.5 (Figs. 2c, S4-5, S8b-d) or 35 meV (in all other figures).

S2. Sample preparation

The Hg1201 single crystals used in this study were grown by a flux method[11] and heat-treated to the desired doping levels[12]. The total mosaic spread of the two primary samples, OP95 (mass ~ 2.0 g) and UD65 (~ 1.8 g), is ~2° FWHM. A third, slightly underdoped crystal (UD89, ~ 1.0 g, mosaic < 0.5°) was studied once in the [H,0,L] plane (Fig. 2b), and was subsequently heat-treated and became part of OP95.

The T_c values of the crystals were measured piece-by-piece using a Quantum Design MPMS instrument (Fig. S1). Quoted T_c values and errors are defined by mid-points and widths of superconducting transitions. Based on our characterization results

(magnetometry and X-ray Laue diffraction), we can rule out the presence of major impurity phase in our samples. We estimate an upper bound of 30 mg of non-Hg1201 phase in sample OP95 (mainly the white Ba-Cu-O phase on the surface of the two largest crystals in Fig. S1), which is less than 2% of the total mass. No noticeable impurity phase was found in sample UD65. Since both the resonance peak at $\mathbf{q}_{AF}$ and the excitation branch (at and away from $\mathbf{q}_{AF}$) were consistently observed in all samples, and given the small volume fraction of the impurity phase and the very large total magnetic spectral weight, the magnetic signal cannot come from the impurity phase. Impurity scattering would also fail to explain the observed temperature dependence that changes with doping and the physically sensible dispersion.

S3. Converting intensities into normalized units

The measurements in this study were carried out on a number of different spectrometers. To compare the intensities in different measurements, we employed a calibration procedure based on Bragg peak intensities measured under the same condition as the inelastic experiments. The amplitude of a Bragg reflection (*H*,*K*,*L*) is:

$$I = C \cdot R_0(H,K,L;\omega = 0) \cdot F_N^{\,2}(H,K,L;\omega = 0),$$

where C is a constant depending on the sample mass and the neutron flux, F_N is the nuclear structure factor, and R_0 is related to the resolution function. R_0 and F_N can be calculated according to instrument configuration and crystal structure, respectively.

Based on the results in Fig. S2, we estimate that the ratio among the $C \cdot R_0$ values for

the three spectrometers is 1:7:21 (IN20: 2T: IN8). In the inelastic measurements, the quantity $C \cdot R_0 \cdot V$ is proportional to the measured intensity of a feature that is weakly dispersing and sharp in energy, where V is the volume of the resolution ellipsoid in momentum space and R_0 needs to be re-calculated for the inelastic condition.

Throughout the manuscript and this SI, the vertical scales in normalized units correspond to a monitor number which takes one minute of measurement time at the energy transfer of 56 meV. We use IN20 as the standard for the conversion to normalized units. Based on Fig. S2 and our resolution calculation, the raw intensities measured on IN8 (using a Cu(200) monochromator, Fig. 2d) and 2T need to be divided by 40 and 7, respectively. On PUMA, due to radiation-protection restrictions, the beam width in the elastic condition has to be reduced from that at high energy transfers, which makes the calibration unfeasible. Nevertheless, given its similar instrument design as 2T and a 40% higher power of the reactor with a compact-core design, we estimate a conversion factor of 10-15 for PUMA. Since actual measurements may involve complications that are not captured by the resolution calculation, we estimate an error of up to 50% in the conversion, which is about the largest percentage discrepancy among the four curves in Fig. S2.

S4. Non-spin-flip measurements for sample OP95

In order to verify that the peaks in Figs. 1a-b are not due to phonon scattering 'leaked' into the spin-flip (SF) channel, scans were carried out in the non-spin-flip (NSF)

channel at 10 K (Fig. S3). Unlike in the SF channel, no systematic feature is observed. Given the high flipping ratio (~15), we conclude that phonon 'leakage' cannot be the cause for the peaks in Figs. 1a-b.

S5. Unpolarized measurements of the dispersion

The measurements were performed on PUMA, with the final neutron energy fixed at 30.5 meV. Energy scans were performed at signal positions $\mathbf{Q}_s = (H,H,6.4)$ for sample UD65. The raw data (filled symbols in Fig. S4a, offset for clarity) clearly show a dispersing feature in the 50-60 meV range, consistent with the results for OP95 (Fig. 1a). To further rule out possible spurious effects and to estimate the background, these scans were complemented with reference scans at background positions $\mathbf{Q}_b = (H',H',0)$ (empty symbols in Fig. S4a). $\mathbf{Q}_b$ was chosen such that $|\mathbf{Q}_s| = |\mathbf{Q}_b|$, in order to minimize the difference in powder scattering and instrumental background between $\mathbf{Q}_s$ and $\mathbf{Q}_b$. Since the $\mathbf{Q}_b$ values are distributed well within the FWHM of the **Q**-resolution, the reference scans were combined to further reduce statistical uncertainty, after confirming that there is no substantial difference among them (Fig. S4b). The dispersion in Fig. 1c is obtained by fitting the background-subtracted data (Fig. S4c) to resolution-limited Gaussian peaks with a common baseline.

For part of sample OP95, a measurement of the excitation away from $\mathbf{q}_{AF}$ was made at $\mathbf{Q} = (0.8,0.8,4.8)$ (Fig. S5). Intensity difference between low and high temperatures reveals the magnetic signal (see ref. 17 for the raw data). A polarized measurement at

this **Q**-position was inconclusive due to the weakness of magnetic signal.

S6. Unpolarized measurements of temperature dependence

The measurement for sample OP95 was performed on 2T. The magnetic excitation away from $\mathbf{q}_{AF}$ is most clearly revealed by the intensity difference between low and high temperatures (Fig. S6b), a method that is commonly employed in neutron scattering studies[19,30-32]. The temperature dependence was measured at the peak position (53 meV) and two candidate background positions (45 and 61 meV) (Fig. S6c). It was then noticed that the intensity at 45 meV increased rapidly at high temperature and was likely affected by phonons. This was confirmed by a careful inspection of the data in Fig. S6a: the blue dashed line (3 K) goes through both candidate background points, whereas the red dashed line (same slope, 295 K) goes through the points at 53 and 61 meV and misses all the points near 45 meV. Therefore, only 61 meV is used as the background. Fitting the intensity difference between 53 and 61 meV to an empirical power-law gives $T_{ex} = 211 \pm 13$ K (Fig. S6d).

The temperature dependence for sample UD65 (Fig. 3a) was similarly measured at **Q** = (0.18,0.18,6.0) at 50, 54 and 60 meV (on IN8, full scans at the lowest and highest temperatures are displayed in Fig. 2d). A power-law fit gives $T_{ex} = 335 \pm 23$ K. For both fits in Fig. 3a, the power-law exponents were empirically fixed to 1.2.

S7. *T** determined by *ab*-plane resistivity

Resistivity data were reported in ref. 12 (T_c = 81 K) and ref. 20 (T_c = 94 K). Here we show additional results for an underdoped sample (T_c ~ 65 K, Fig. S7). We follow the widely-accepted convention of extracting T^*, defined as the temperature below which the in-plane resistivity deviates considerably from an approximately linear behavior at higher temperatures. We estimate a conservative uncertainty of 25 K on T^*.

S8. The resonance at $\mathbf{q}_{AF}$ in Hg1201

Additional data for the resonance are presented in Fig. S8. The resonance peak is centered at $\mathbf{q}_{AF}$ and does not extend to $q = 0$ (momentum width consistent with those in YBCO and Tl2201, see discussion in ref. 17). At energies above and below 56 meV, a weak signal centered at $\mathbf{q}_{AF}$ is observed, which is similar to the situation near the resonance in other cuprates, and which might be the counterpart of the 'hourglass' excitations in Hg1201. The limited statistical accuracy does not allow us to determine whether the response below and above the resonance energy is commensurate.

S9. How could the excitation branch have been missed so far?

To the authors' knowledge, there exist no reports in the literature of the cuprate superconductors of spin-polarized INS measurements at momentum positions near the 2D zone center, and especially not of measurements involving energy scans near the 2D zone center. As demonstrated by our results for Hg1201, such scans reveal the excitation branch most clearly. The lack of such measurements is partly due to the fact that the main focus of the previous polarized measurements had been to confirm

unpolarized results for the antiferromagnetic response, especially the resonance at $\mathbf{q}_{AF}$ (ref. 16). This response is best measured with momentum scans at constant energy[33-35], or with energy scans at $\mathbf{q}_{AF}$ (refs. 35,36), but not with energy scans near $q = 0$.

Unpolarized measurements, which are much more common, inevitably contain both phonon and magnetic contributions. Phonon signals can be strong, and they may stem not only from the sample, but also from the sample mount (usually made of aluminum). Therefore, it is common practice to ignore 'bumps' in raw data of unpolarized energy scans that have no obvious connection to the response at $\mathbf{q}_{AF}$. For the same reason, momentum scans were regarded as more useful, because (weakly-dispersive) optical phonons are expected to only contribute to the 'background.' While this is true when the signal of interest is peaked at specific **Q**-positions (such as $\mathbf{q}_{AF}$), the magnetic excitation branch reported here would unfortunately also only contribute to the presumed 'background'. Such 'background' in momentum scans (or in constant-energy slices in time-of-flight measurements) was either removed or received little attention when data at different energies were compared (for example, see refs. 14,15,19,28,32,37-41).

One way of extracting magnetic signal from unpolarized data is to compare scans at different temperatures. With increasing temperature, phonon intensities tend to increase due to the Bose factor, whereas magnetic signals tend to decrease. Even though the effects of phonons and of magnetic excitations might cancel each other,

there is still a chance to extract the latter if the correct type of scan is used. This has been one of our main approaches to measure the excitation branch using unpolarized neutrons. However, just as for energy scans near the 2D zone center with polarized neutrons, we did not find any comparison in the literature between energy scans at small H and K values at different temperatures. Moreover, the excitation branch reported here sets in near T^*, but comparisons that received most attention previously were for temperatures across T_c (refs. 19,30,32,34,38,42-44). Such comparisons were optimized to highlight the resonance, but might have missed a substantial part of the intensity change due to the excitation branch. In fact, this focus on the intensity change across T_c had prevented the community from realizing the importance of the normal-state response near $\mathbf{q}_{AF}$ (refs. 15,37,45) until long after the resonance was discovered. The situation is similar in our case. A hint of the excitation branch was serendipitously observed when we measured the resonance in Hg1201 (ref. 17) and compared data at 10 K and room temperature (rather than just above T_c), and this observation motivated the present work. The high resonance energy in Hg1201 has provided an advantage in this regard, because the Bose factor change between 10 K and 300 K for 55 meV is only half of that for 40 meV, the approximate energy of the (odd-party) resonance energy in YBCO. Had the excitation branch been at ~ 40 meV, *i.e.*, close to the odd-parity resonance energy in double-layer systems, it would have been more difficult to discern, because the effect could have been more easily hidden by the increase of phonon scattering due to the Bose factor.

One might think that time-of-flight measurements should have accidentally revealed the excitation branch, because a large portion of the momentum-energy space is mapped out in such measurements without selective focus. However, such measurements have several drawbacks as well. First, the commonly used sample orientation (*c*-axis along beam axis) does not allow access to $H = K = 0$, where the excitation branch gives the strongest signal. Second, the 'background' is hardly understood and generally ignored. Third, the signal intensity at a given momentum-energy position is low, which makes careful studies on the temperature dependence very time consuming. Finally, to date, detailed spin-polarization analysis has not been possible with time-of-flight spectrometers.

The excitation might be particularly difficult to observe in $La_{2-x}Sr_xCuO_4$, one of the most intensively studied cuprates. In this compound, the unusual magnetic order was recently found to be very short-ranged[46], either because of competing stripe order[47] or strong disorder effects[13], which can be expected to lead to highly damped (broad in energy) excitations that are difficult to detect.

References:

30. He, H. *et al.* Magnetic resonant mode in the single-layer high-temperature superconductor $Tl_2Ba_2CuO_{6+\delta}$. *Science* **295**, 1045-1047 (2002).

31. Wilson, S. D. *et al.* Resonance in the electron-doped high-transition-temperature superconductor $Pr_{0.88}LaCe_{0.12}CuO_{4-\delta}$. *Nature* **442**, 59 (2006).

32. Woo, H. *et al.* Magnetic energy change available to superconducting condensation in optimally doped $YBa_2Cu_3O_{6.95}$. *Nat. Phys.* **2**, 600-604 (2006).

33. Fong, H. F. *et al.* Superconductivity-induced anomalies in the spin excitation spectra of underdoped $YBa_2Cu_3O_{6+x}$. *Phys. Rev. Lett.* **78**, 713-716 (1997).

34. Dai, P. *et al.* Evolution of the resonance and incommensurate spin fluctuations in superconducting $YBa_2Cu_3O_{6+x}$. *Phys. Rev. B* **63**, 054525 (2001).

35. Dai, P. *et al.* Magnetic dynamics in underdoped $YBa_2Cu_3O_{7-x}$: Direct observation of a superconducting gap. *Phys. Rev. Lett.* **77**, 5425-5428 (1996).

36. Mook, H. A. *et al.* Polarized neutron determination of the magnetic excitations in $YBa_2Cu_3O_7$. *Phys. Rev. Lett.* **70**, 3490-3493 (1993).

37. Dai, P. *et al.* The magnetic excitation spectrum and thermodynamics of high-T_c superconductors. *Science* **284**, 1344-1347 (1999).

38. Reznik, D. *et al.* Dispersion of magnetic excitations in optimally doped superconducting $YBa_2Cu_3O_{6.95}$. *Phys. Rev. Lett.* **93**, 207003 (2004).

39. Stock, C. *et al.* From incommensurate to dispersive spin-fluctuations: The high-energy inelastic spectrum in superconducting $YBa_2Cu_3O_{6.85}$. *Phys. Rev. B* **71**, 024522 (2005).

40. Wakimoto, S. *et al.* Disappearance of antiferromagnetic spin excitations in overdoped $La_{2-x}Sr_xCuO_4$. *Phys. Rev. Lett.* **98**, 247003 (2007).

41. Reznik, D. *et al.* Local-moment fluctuations in the optimally doped high-T_c superconductor $YBa_2Cu_3O_{6.95}$. *Phys. Rev. B* **78**, 132503 (2008).

42. Bourges, P. *et al.* Inelastic-neutron-scattering study of antiferromagnetic

fluctuations in $YBa_2Cu_3O_{6.97}$. *Phys. Rev. B* **53**, 876-885 (1996).

43. Fong, H. F. *et al.* Neutron scattering from magnetic excitations in $Bi_2Sr_2CaCu_2O_{8+\delta}$. *Nature* **398**, 588-591 (1999).

44. Xu, G. *et al.* Testing the itinerancy of spin dynamics in superconducting $Bi_2Sr_2CaCu_2O_{8+\delta}$. *Nat. Phys.* **5**, 642-646 (2009).

45. Stock, C. *et al.* Dynamic stripes and resonance in the superconducting and normal phases of $YBa_2Cu_3O_{6.5}$ ortho-II superconductor. *Phys. Rev. B* **69**, 014502 (2004).

46. Balédent, V. *et al.* 2D orbital-like magnetic order in $La_{2-x}Sr_xCuO_4$. arXiv: 1005.3406.

47. Tranquada, J. M. *et al.* Evidence for stripe correlations of spins and holes in copper oxide superconductors. *Nature* **375**, 561-563 (1995).

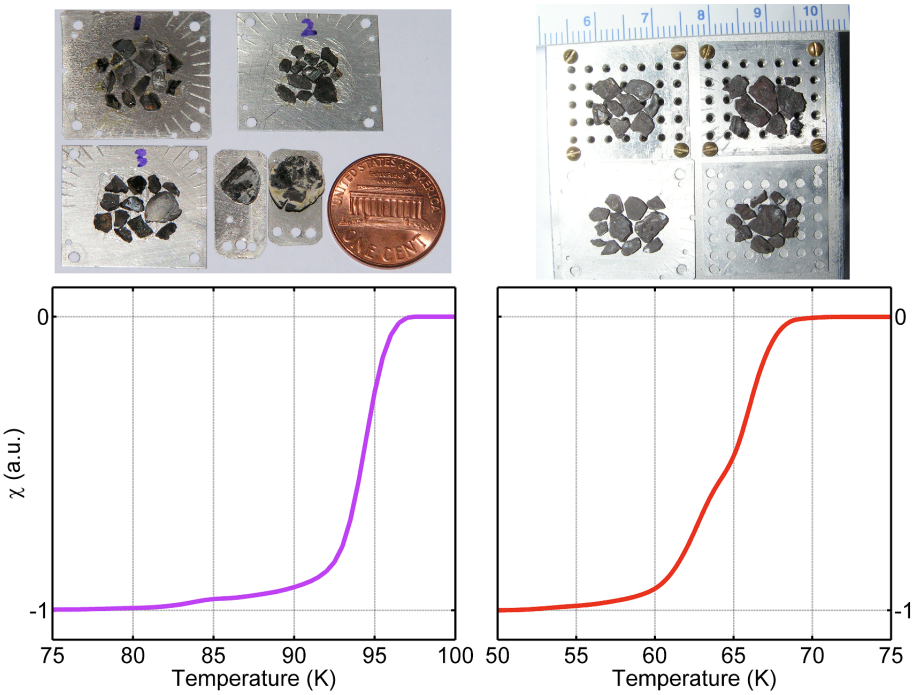

Figure S1. Pictures and summed magnetometry curves for the two primary samples: OP95 (left) and UD65 (right).

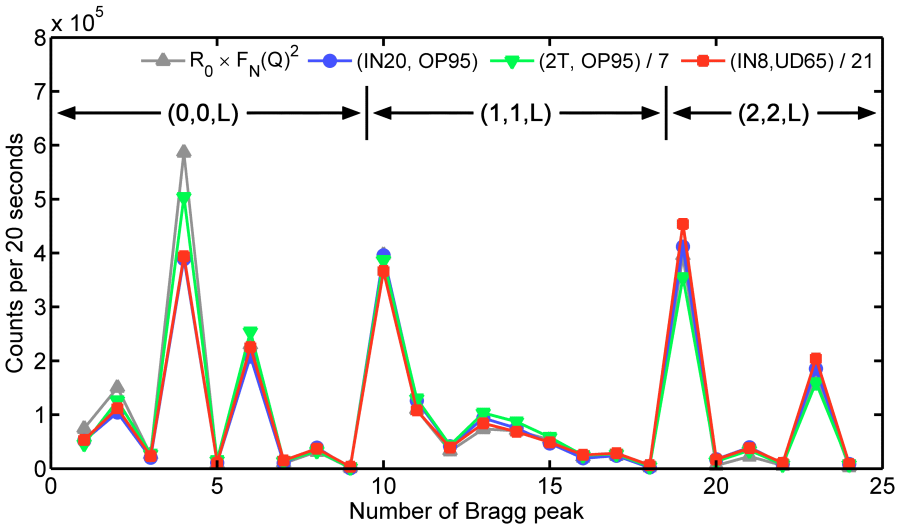

Figure S2. Nuclear Bragg peak intensity measured on (001) to (009), (110) to (118) and (220) to (225), labeled as numbers 1 to 24, for three spectrometers. Also plotted are the (rescaled) product of the calculated R_0 values for spectrometer IN20 and $F(Q)^2$ for the Bragg reflections. The overall agreement demonstrates that the three spectrometers have similar (and regular) resolution functions, and that the intensity difference can be approximated by the single quantity $C \cdot R_0$. The calculated R_0 values of other spectrometers have similar ratios among the different reflections, and are therefore not shown.

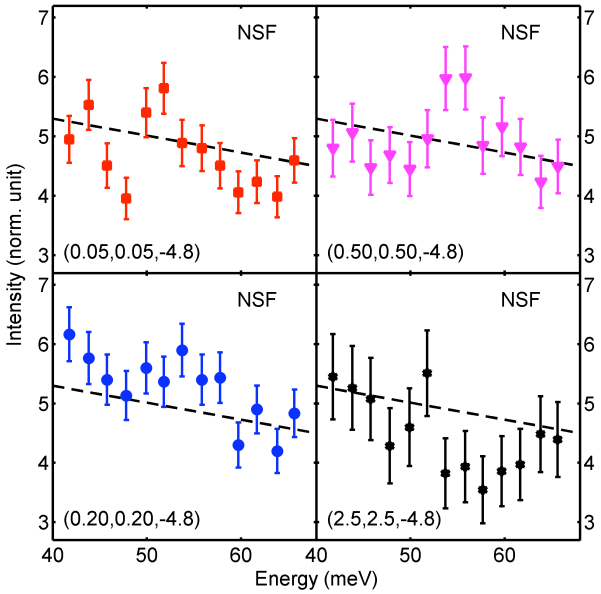

Figure S3. Non-spin-flip energy scans for sample OP95 at the same **Q**-positions as in Figs. 1a-b at $T = 10$ K (measured on IN20). An identical dashed line is drawn in all panels to facilitate comparison among the panels. The absence of peak at $H = 2.5$ rules out a phonon interpretation of a possible feature at $H = 0.5$. Error bars indicate statistical uncertainty (one standard deviation).

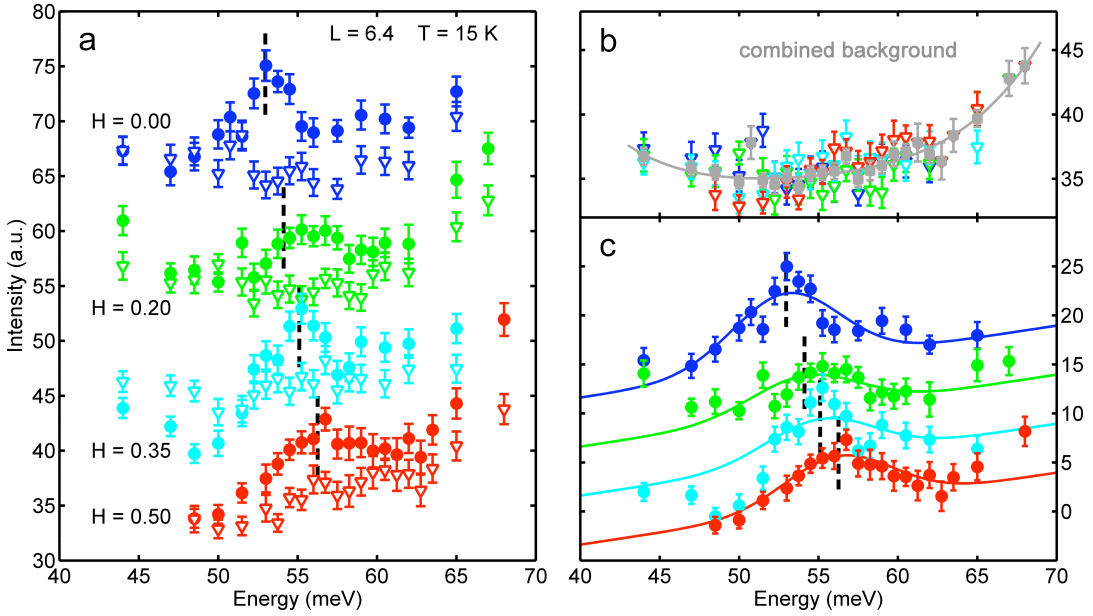

Figure S4. (**a**) Unpolarized energy scans for sample UD65 at (*H*,*H*,6.4) (filled circles) and corresponding $\mathbf{Q}_b$-positions (empty triangles, see text). The choice of positive *L* is in accordance with the configuration of the PUMA instrument, so that the resolution ellipsoid has a momentum-energy space orientation similar to that on IN20 with negative *L*. (**b**) The reference scans are combined and described by a polynomial (grey line). (**c**) Background-subtracted data fit by resolution-limited (9.5 meV FWHM) Gaussian. Vertical scales correspond to one minute of measurement time at 56 meV (before conversion to normalized units). Data in (a) and (c) are offset for clarity. Vertical dashed lines indicate the fit peak positions. Error bars indicate statistical uncertainty (one standard deviation).

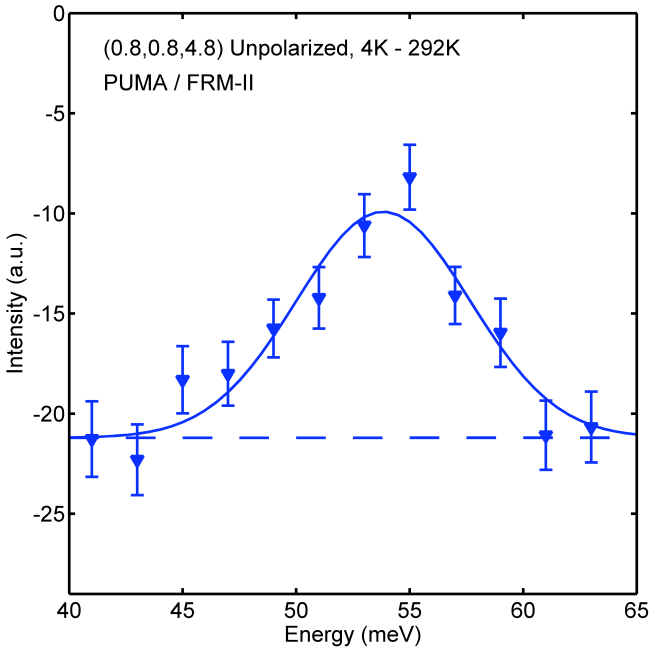

Figure S5. Unpolarized measurement on PUMA for part of sample OP95. The solid line is a resolution-limited (9.5 meV FWHM) Gaussian fit to the data. Error bars indicate statistical uncertainty (one standard deviation).

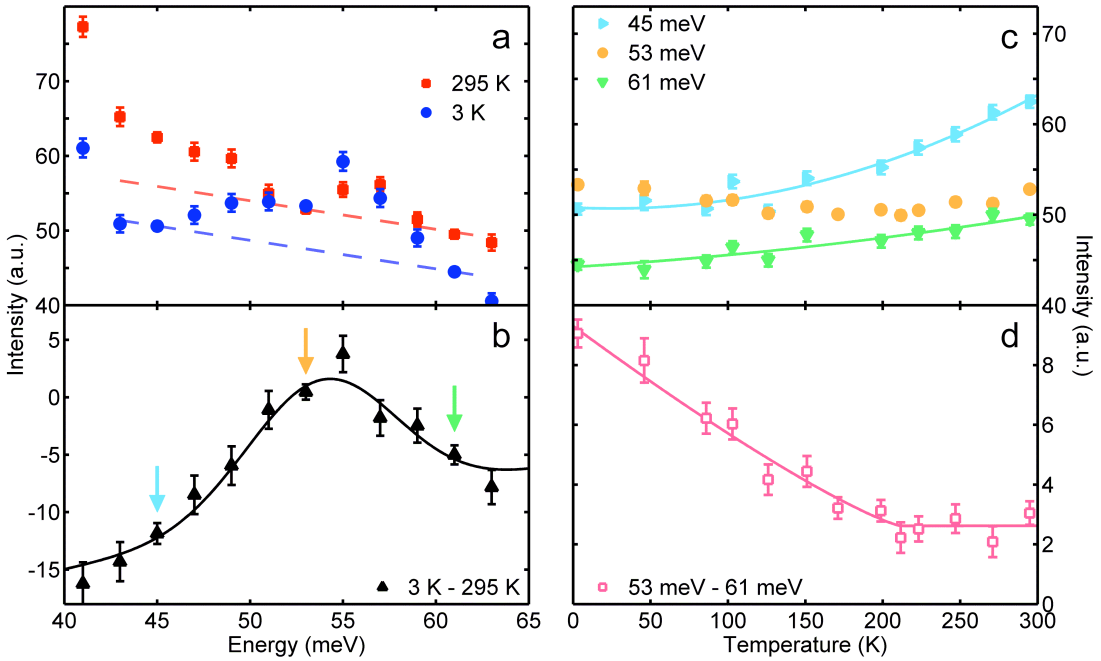

Figure S6. (**a**) Unpolarized energy scans at **Q** = (0.2,0.2,5.2) for OP95. The choice of positive L is in accordance with the configuration of the 2T instrument, so that the resolution ellipsoid has a momentum-energy space orientation similar to that on IN20 with negative L. The dashed lines are for comparing the background levels and have the same slope (see text). (**b**) Intensity difference between 3 K and 295 K, fit to a resolution-limited (9 meV) Gaussian (center 53.8 ± 0.9 meV) on a sloping baseline. (**c**) Temperature dependencies at the arrowed positions in (b). The lines are quadratic smoothing curves. (**d**) Difference between 53 meV data and the smoothing curve for 61 meV in (c). An empirical power-law fit (solid line) gives an onset temperature of T_{ex} = 211 ± 13 K. Vertical scales correspond to one minute of measurement time at 56 meV (before conversion to normalized units). Error bars indicate statistical uncertainty (one standard deviation).

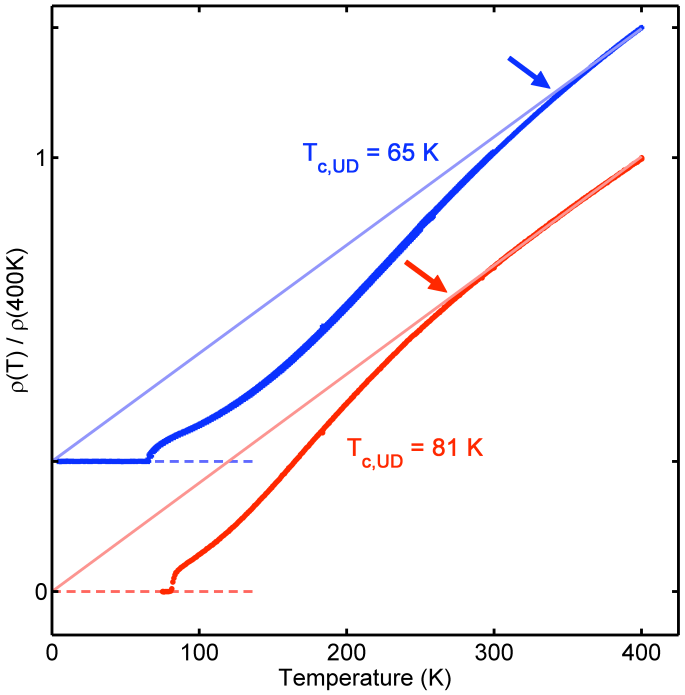

Figure S7. In-plane DC resistivity measurements of underdoped Hg1201 single crystals using the standard 4-probe method[12]. The thin lines are linear fits to the data above 300 K and 350 K for the T_c ~ 81 K and ~ 65 K samples, respectively. Values of T^* (268 K and 338 K) defined by considerable deviation from an approximately linear behavior are indicated by the arrows.

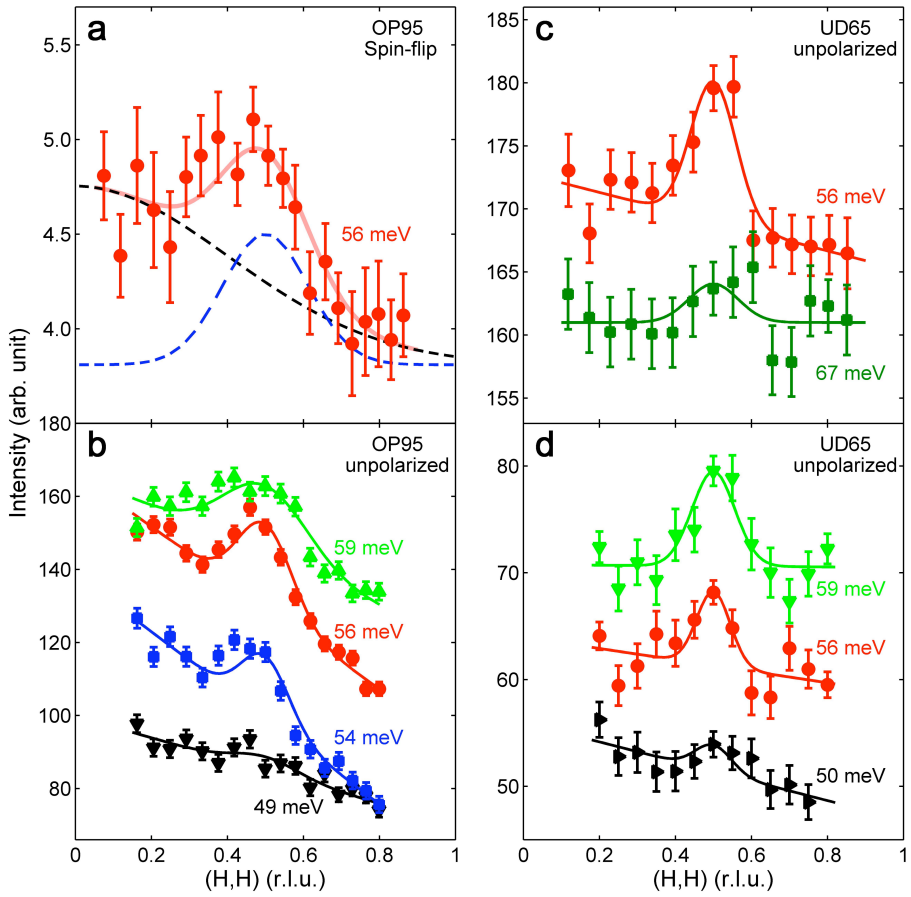

Figure S8. Momentum scans at $T < 15$ K. (**a**) Spin-flip data for sample OP95 showing the resonance at $\mathbf{q}_{AF}$ (blue dashed line) together with the excitation centered at $q = 0$ (black dashed line). The scan was performed by rocking the sample (keeping Q constant) through (0.5,0.5,-4.0). (**b**) Unpolarized rocking scans for OP95 at several energies near the resonance. Data are offset for clarity. Adapted from ref. 17. (**c-d**) Unpolarized momentum scans for UD65. The measurements in the two panels were performed using different configurations. Data are offset for clarity.